Atmos. Meas. Tech., 9, 509–524, 2016
www.atmos-meas-tech.net/9/509/2016/
doi:10.5194/amt-9-509-2016

Atmospheric Measurement Techniques
Open Access
EGU

A dual-inlet, single detector relaxed eddy accumulation system for long-term measurement of mercury flux

S. Osterwalder[1], J. Fritsche[1], C. Alewell[1], M. Schmutz[1], M. B. Nilsson[2], G. Jocher[2], J. Sommar[3], J. Rinne[4,5], and K. Bishop[6,7]

[1]Department of Environmental Sciences, University of Basel, Basel, Switzerland
[2]Department of Forest Ecology and Management, Swedish University of Agricultural Sciences, Umeå, Sweden
[3]State Key Laboratory of Environmental Geochemistry, Chinese Academy of Sciences, Guiyang, China
[4]Department of Geosciences and Geography, University of Helsinki, Helsinki, Finland
[5]Finnish Meteorological Institute, Helsinki, Finland
[6]Department of Aquatic Sciences and Assessment, Swedish University of Agricultural Sciences, Uppsala, Sweden
[7]Department of Earth Sciences, University of Uppsala, Uppsala, Sweden

Correspondence to: S. Osterwalder (stefan.osterwalder@unibas.ch)

Received: 5 June 2015 – Published in Atmos. Meas. Tech. Discuss.: 5 August 2015
Revised: 31 December 2015 – Accepted: 18 January 2016 – Published: 15 February 2016

Abstract. The fate of anthropogenic emissions of mercury (Hg) to the atmosphere is influenced by the exchange of elemental Hg with the earth surface. This exchange holds the key to a better understanding of Hg cycling from local to global scales, which has been difficult to quantify. To advance research about land–atmosphere Hg interactions, we developed a dual-inlet, single detector relaxed eddy accumulation (REA) system. REA is an established technique for measuring turbulent fluxes of trace gases and aerosol particles in the atmospheric surface layer. Accurate determination of gaseous elemental mercury (GEM) fluxes has proven difficult due to technical challenges presented by extremely small concentration differences (typically $< 0.5\,\mathrm{ng\,m^{-3}}$) between updrafts and downdrafts. We present an advanced REA design that uses two inlets and two pairs of gold cartridges for continuous monitoring of GEM fluxes. This setup reduces the major uncertainty created by the sequential sampling in many previous designs. Additionally, the instrument is equipped with a GEM reference gas generator that monitors drift and recovery rates. These innovations facilitate continuous, autonomous measurement of GEM flux. To demonstrate the system performance, we present results from field campaigns in two contrasting environments: an urban setting with a heterogeneous fetch and a boreal peatland during snowmelt. The observed average emission rates were 15 and $3\,\mathrm{ng\,m^{-2}\,h^{-1}}$, respectively. We believe that this dual-inlet, single detector approach is a significant improvement of the REA system for ultra-trace gases and can help to advance our understanding of long-term land–atmosphere GEM exchange.

1 Introduction

The UN's legally binding Minimata Convention has been signed by 128 countries since October 2013 and aims to protect human health and welfare by reducing anthropogenic release of mercury (Hg) into the environment (UNEP, 2013a). Current anthropogenic sources, mainly from fossil fuel combustion, mining, waste incineration and industrial processes, are responsible for about 30 % of annual Hg emissions to the atmosphere. Additional 10 % comes from natural geological sources and the remaining 60 % from re-emission of previously deposited Hg (UNEP, 2013b). As a result, long-range atmospheric transport of gaseous elemental mercury (GEM or Hg^0) has led to Hg deposition and accumulation in soils and water bodies well in excess of natural levels even in remote areas, far away from anthropogenic pollution sources (Grigal, 2002; Slemr et al., 2003).

Quantification of Hg emission and deposition is needed to reduce the large gaps that exist in the global Hg mass balance estimates (Mason and Sheu, 2002) and as a basis of legisla-

tion targeting the control of Hg emissions (Lindberg et al., 2007). Gustin et al. (2008) suggest that today a substantial amount of Hg deposited on soils with natural background concentrations of Hg ($< 0.1\ \mu g\ g^{-1}$) is re-emitted back to the atmosphere and that over the course of a year deposition is largely compensated for by re-emission, resulting in a net flux close to 0.

The state of the art in field techniques to quantify Hg flux from terrestrial surfaces has been summarized in review papers (Gustin, 2011; Gustin and Lindberg, 2005; Gustin et al., 2008; Sommar et al., 2013b; Agnan et al., 2016). They conclude that environmental, physicochemical and meteorological factors as well as surface characteristics determine the accuracy and precision of GEM flux measurements. Fluxes are commonly determined using dynamic flux chambers (DFCs) or micrometeorological techniques (relaxed eddy accumulation (REA), modified Bowen ratio (MBR) or the aerodynamic gradient (AGM) method). DFCs are the most widely used technique to measure in situ GEM fluxes since they are easy to handle and inexpensive. However, DFCs alter the enclosed environment of the volume and surface area being studied by affecting atmospheric turbulence, temperature and humidity (Wallschläger et al., 1999; Gillis and Miller, 2000; Eckley et al., 2010). Also the concern about influencing plant physiology means that DFCs are restricted to short-term measurements and studies comparing the relative differences between sites only, e.g., control and treatment experiments (Fritsche et al., 2014).

A major advantage of micrometeorological techniques is that they are conducted under conditions with minimal disturbance. As they can be applied continuously, they provide flux data valuable to characterize ecosystems as sinks or sources of atmospheric Hg and to interpret seasonal flux patterns. Micrometeorological techniques are also able to cover a much larger area than DFC techniques, although this larger "footprint" should be relatively flat and homogeneous. Several studies report results from GEM land–atmosphere exchange measurements over a variety of landscapes using MBR and AGM techniques (e.g., Kim et al., 1995; Meyers et al., 1996; Gustin et al., 2000; Lindberg and Meyers, 2001; Fritsche et al., 2008b; Converse et al., 2010). Fritsche et al. (2008a) concluded that micrometeorological techniques are appropriate to estimate Hg exchange rates but often suffered from large uncertainties due to extremely low concentration gradients over background soils. Eddy covariance (EC) has the potential to detect high-frequency atmospheric GEM concentration fluctuations and might improve flux estimates considerably (Bauer et al., 2002; Faïn et al., 2010). Pierce et al. (2015) conducted the first successful EC flux measurements of GEM over Hg-enriched soils measuring atmospheric GEM concentrations at high frequency (25 Hz). However, on background soils measured fluxes were below the detection limit.

To overcome the need for fast-response sensors, Desjardins (1977) has introduced the eddy accumulation method where fast-response sampling valves are combined with slow analysis techniques on the assumption that the turbulent covariance flux can be averaged separately for positive and negative vertical wind velocities. The technical breakthrough for REA was achieved by Businger and Oncley (1990), simulating the method with vertical wind, temperature and humidity time series in the surface layer. The main advantage of REA over other micrometeorological methods is that REA requires sampling at only one height and therefore flux divergence may be measured directly (Sutton et al., 2001). Reactive substances can be lost by chemical reaction between two sampling heights (Olofsson et al., 2005a; Foken, 2006; Fritsche et al., 2008a), and sensors at two heights also have different footprints. REA eliminates these drawbacks (Bash and Miller, 2008). There are disadvantages to be considered as well though. The technical requirements for REA are very stringent, increasing the demand on the precision of the sampling and chemical analysis. Irregularities in offset measurements and timing of the sampling valves can also not be corrected for later (Sutton et al., 2001).

The REA method has been widely used since 1990 to investigate fluxes of different trace gases and aerosols (e.g., Brut et al., 2004; Gaman et al., 2004; Olofsson et al., 2005a; Haapanala et al., 2006; Arnts et al., 2013). This includes a few applications on land–atmosphere GEM exchange over soils (Cobos et al., 2002; Olofsson et al., 2005b; Sommar et al., 2013a; Zhu et al., 2015a) and forest canopies (Bash and Miller, 2007, 2008, 2009). Additionally, reactive gaseous Hg fluxes have been measured over snow surfaces in the Arctic (Skov et al., 2006). Besides valuable data of net exchange rates of GEM over different environments, the studies have also identified potential for refinement in the technical implementation of REA. The dual detector system presented by Olofsson et al. (2005b) was criticized since it suffered from inherent variability and drift of sensitivity between the two Hg detectors (Sommar et al., 2013a). Sommar et al. (2013a) modified the systems employed by Cobos et al. (2002) and Bash and Miller (2008) to create a single-inlet REA system. However, their system lacks the capability to accumulate samples from the up- and downdraft channels synchronously. The application of sequential measurement of the channels impairs the accuracy with which fluxes can be gauged when the concentration of atmospheric GEM varies on the scale of the sampling period (Zhu et al., 2015b).

Even though there has been steady improvement in REA systems for measuring GEM fluxes, the financial and technical challenges to accurately measure the extremely low concentration differences (sub-ppt range) in up- and downdrafts have limited the number of studies (Foken, 2006). Thus, there remains a demand for a system especially designed to continuously monitor background GEM fluxes with minimum maintenance requirements.

To address these needs we designed a fully automated REA system with two inlet lines for continuous air sampling. The GEM contained in these samples is collected on a pair of

gold cartridges: with one for updraft and the other for downdraft. Two such pairs of gold cartridges are used, with one pair collecting GEM while the other pair is analyzed on a single Hg detector, one cartridge after the other. To detect any instrument drift, contamination and changes in GEM recovery, the system is equipped with a GEM reference gas generator and a Hg zero-air generator.

Our objective was to develop an advanced REA system that reduces the major measurement uncertainty of earlier systems created by sequential sampling procedures. We achieved this goal by

1. continuous, simultaneous sampling of GEM in up- and downdrafts using two pairs of gold cartridges;
2. regular analysis of a GEM reference gas as well as dry, Hg-free air to monitor accurate GEM quantification;
3. fully automated air sampling and GEM analysis with an online user interface that provides comprehensive information about system performance.

To test the system's performance under field conditions, we deployed it in two contrasting environments during campaigns of 2 to 3 weeks each. At the first site in the center of Basel, Switzerland, GEM fluxes were measured 20 m above the roof of a building, 39 m above ground level. Later on the system was installed 1.8 m above a boreal peatland called Degerö in northern Sweden during snowmelt.

This paper includes a description of the novelties in the REA design and presents a time series of GEM flux measurements from each of the deployments with contrasting atmospheric conditions and site characteristics. To analyze the system performance we compared source–sink characteristics using footprint models and analyzed turbulence regimes to determine possible flux attenuation. We briefly discuss several instrumental factors which might affect the accuracy of the flux measurements: bias in vertical wind measurements, control and response time of the REA sampling valves, measurement precision of the sample volumes as well as the performance of analytical schemes and calibration procedures. Furthermore, we describe the evaluation of the β constant, the method detection limit and rejection criteria for flux measurements based on the REA validation procedure.

2 Materials and methods

2.1 GEM-REA sampling system

The concept of our advanced REA design is based on a GEM sampling unit with two pairs of gold cartridges, a single Hg detector as well as a GEM reference gas generator and a zero-air generator. Figure 1 illustrates the setup of the sampling and analysis system. Table S1 in the Supplement lists the major components. Both study sites are equipped with continuously operating EC systems that have been measuring sensible and latent heat flux and CO_2 exchange at 30 min intervals

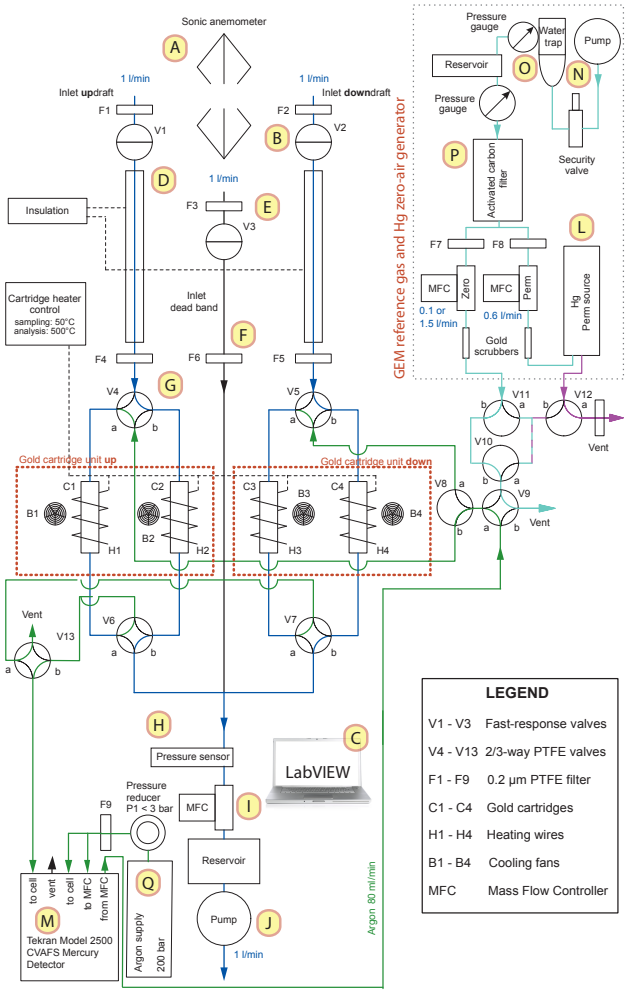

Figure 1. Schematic of the REA system hardware. It consists of a GEM sampling unit, a GEM reference gas generator and a Hg zero-air generator (upper right). Capital letters refer to REA components mentioned in the text and described in Table S1. The air volume drawn over the gold cartridges equaled 1 L min^{-1} in Basel and 1.5 L min^{-1} at Degerö.

(Sagerfors et al., 2008; Lietzke and Vogt, 2013) for many years. A suite of meteorological parameters were recorded as well: solar radiation, air and soil temperature, relative humidity, precipitation, snow depth, wind speed and direction, friction velocity and surface layer stability parameters.

Vertical wind velocity GEM flux quantification was measured with a 3-D sonic anemometer (10 Hz) (A1, A2). The wind signal was transferred to three fast-response switching solenoid valves (B) via LabVIEW (C) enabling sampling and separation of air into updraft, downdraft and deadband channels. The fast-response valves were installed 0.2 m downstream of the sampling inlets. The inlets of the 1/4″ PTFE sampling lines (D) were mounted near the anemometer head about 15 cm below the midpoint of the ultrasonic paths.

GEM carried in the "updrafts" and "downdrafts" was then collected on two pairs of gold cartridges. The flux (ng m^{-2} h^{-1}) was calculated from the GEM concentration difference (ng m^{-3}) in updraft ($\overline{C_u}$) and downdraft ($\overline{C_d}$) air, multiplied by σ_w (m s^{-1}), the standard deviation of vertical wind velocity.

$$F_{GEM} = \beta\sigma_w(\overline{C_u} - \overline{C_d}) \quad (1)$$

β is the unitless flux proportionality coefficient and depends on the wind velocity deadband (see Sect. 3.1.2) that is implemented to increase the concentration difference. β values typically range between 0.4 and 0.6. Deadband widths (m s^{-1}) used in recent REA measurement studies ranged from 0.33 to 0.6 times σ_w (Grönholm et al., 2008).

During the campaign in Basel larger eddies resulted in lower valve switching frequencies relative to the situation at Degerö. The atmospheric GEM concentration differences between updraft and downdraft were also larger in Basel. This made the fixed deadband appropriate for Basel, while a dynamic deadband was more favorable for Degerö. A fixed deadband makes β dependent on atmospheric conditions (Milne et al., 1999, 2001), with increased deadband widths leading to lower β values (Ammann, 1999). The application of a dynamic deadband at Degerö, with its smaller eddies, aimed to reduce the switching frequency of the fast-response valves. Using a dynamic deadband also ensured that large enough air volumes for the GEM analysis were measured that would not have been guaranteed by measuring with a fixed deadband. A dynamic deadband is applied more often (cf. Gaman et al., 2004; Olofsson et al., 2005b; Haapanala et al., 2006; Ren et al., 2011) and enables the use of a constant β (Grönholm et al., 2008).

β was calculated from the sonic temperature for each 30 min period at the same intervals used for the "up" and "down" GEM sampling system:

$$\beta = \frac{(\overline{w'T'})}{\sigma_w(\overline{T_u} - \overline{T_d})}, \quad (2)$$

where $\overline{T_u}$ and $\overline{T_d}$ are the "up" and "down" averages of temperature and $\overline{w'T'}$ is the average EC sensible heat flux. In our application a recursive high-pass filter was implemented to reduce low-frequency bias in turbulent time series of the vertical wind velocity (McMillen, 1988; Richardson et al., 2012):

$$\chi_i = \alpha\chi_{i-1} + (1-\alpha)\chi, \quad (3)$$

where χ_i is the filtered value, χ_{i-1} is the running mean from the previous time step and χ is the current, instantaneous value (Meyers et al., 2006).

$$\alpha = e^{-\frac{\Delta t}{\tau}} \quad (4)$$

The constant α results from the sampling interval of 10 Hz (Δt) and the time constant (τ), which was set to 1000 s.

The sampling lines were 20 m long and insulated to avoid condensation. PTFE filters (E, F) of 0.2 µm were installed after the inlets and before the PTFE valves, V4 and V5 (G). The resistance through the sampling lines was checked to be equal using thermal mass flow meters (Vögtlin Instruments AG, Switzerland). Conditionally sampled GEM is subsequently accumulated on two matched pairs of gold cartridges (Tekran Inc., Canada; difference between cartridge sensitivity < 5 % according to manufacturing tests by the supplier). Heating wires around the cartridges were kept at 50 °C during the sampling phase and heated to 500 °C during the desorption process (see Sect. 2.2). Downstream, a pressure sensor (H) operating at 10 Hz was installed to monitor pressure fluctuations. A high-precision thermal mass flow controller (MFC) (I) with a response time of 50 ms was used to regulate the air volume drawn over the gold cartridges. To dampen sampling flow disturbances a reservoir of 200 mL was installed between the pump and the MFC. Air was drawn through the three lines by a rotary vane pump (J) at a rate of 1 L min^{-1} (Basel) and 1.5 L min^{-1} (Degerö), respectively. Three temperature-controlled, weatherproof boxes (K) contained the GEM reference gas generator (L) and Hg detector (M), the gold cartridge unit and the control system as well as the Hg zero-air generator to produce dry, Hg-free air. Remote control of the system allowed online checks of the data and detection of instrumental failures.

2.2 GEM analysis

Air sampling and GEM analysis was performed in parallel in 30 min intervals (Fig. 2). GEM in air samples and injections from the GEM reference gas and Hg zero-air generator were quantified using cold vapor atomic fluorescence spectrophotometry (M). The temperature-controlled GEM reference gas generator provided precise GEM concentrations in a constant stream of dry, Hg-free air. The average recovery of the GEM standard was determined by back calculation from the manual calibration of the Hg detector. The average ± SD loading on cartridge pair 2–4 corresponded to 27.2 ± 1.1 and 22.2 ± 1.3 pg in Basel and 32.1 ± 2.1 and 32.1 ± 2.3 pg at Degerö. Dry, Hg-free air was generated using an air compressor (N) with air dryer (O) and an activated carbon filter (P). Additional gold mercury scrubbers were installed at the outlet of the Hg zero-air generator.

Figure 2 illustrates the sampling and analysis sequence. Upon startup cartridges C2 and C4 are in the air sampling mode, while GEM previously collected on C1 and C3 is analyzed. During the first 5 min GEM of the idle cartridges is desorbed by heating the cartridges to 500 °C in a stream (80 mL min^{-1}) of high-purity Argon (Ar) carrier gas (Q). The cartridge analysis procedure for individual samples included five steps: Ar flushing (20 s), recording baseline (10 s), cartridge heating (28 s), peak delay (30 s) and cooling of the cartridges (60 s). After up- and downdraft air samples had been analyzed (Aa), the cartridges were loaded for 5 min

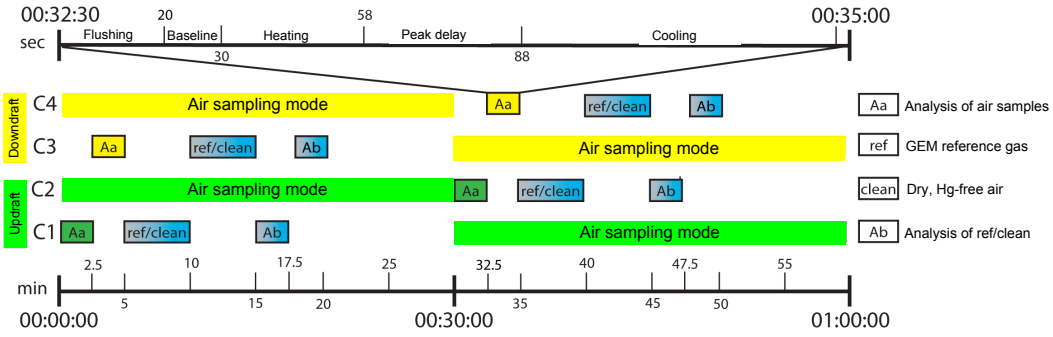

Figure 2. The hourly measuring cycle of the REA system subdivided into the air sampling and GEM analysis procedures (Aa, ref/clean, Ab). At the start of a sequence, cartridge pair C2 and C4 adsorb GEM in the up- and downdraft simultaneously while previously adsorbed GEM from cartridges C1 and C3 is analyzed. During each cycle, eight analysis procedures which last for 2.5 min were conducted.

each with either GEM reference gas (ref) or dry, Hg-free air (clean). The flow rate of dry, Hg-free air (carrier gas) through the GEM reference gas generator was set to 600 mL min^{-1} using a MFC. The GEM reference gas was pre-mixed with 100 mL min^{-1} dry, Hg-free air before being supplied to the cartridges. Dry, Hg-free air was delivered at a flow rate of 1500 mL min^{-1} regulated by another MFC. The cartridges loaded with ref/clean air were analyzed (Ab phase in Fig. 2) following the same procedure as the air samples.

The average and standard deviation of the Hg detector baseline were calculated for periods of three seconds before and after the Hg peak. The baseline below the peak was interpolated and subtracted from the peak. The peak areas were logged together with 30 min averages of the sampled air volume, opening times and number of switching operations of the fast-response valves. Air temperatures within the weatherproof boxes, Hg detector lamp- and UV sensor voltages as well as pressure sensor data were also recorded.

2.3 QA/QC

2.3.1 Calibration of Hg detector

The REA system was calibrated after the field campaigns using a temperature-controlled Hg vapor calibration unit (R) together with a digital syringe (S). Different concentrations of saturated GEM vapor were injected into the Hg-free air stream provided by a Hg zero-air generator (T). During calibration a simulated wind signal was used to supply both lines with an equal amount of air. Calibration factors were gained by linear regression between the injected quantity of GEM and observed peak areas (Fig. S1).

2.3.2 Monitoring of GEM recovery

Repeated injections from the GEM reference gas and Hg zero-air generator (Fig. 2) were performed to observe possible contamination, passivation or drift of the cartridges, as well as to check for temperature sensitivity in the Hg detector. Before and after a measurement campaign the system was checked for leaks by measuring dry, Hg-free air from the Hg zero-air generator and by constricting the sampling lines temporarily to check for pressure decrease within the lines. PTFE parts and tubing were cleaned with 5 % nitric acid according to a standard operating procedure (adapted from Keeler and Landis, 1994).

2.3.3 Bias of sampling lines

To assess potential systematic bias between up- and downdraft sampling lines, GEM reference gas was supplied to both lines. During 5 days in Basel and 28 h at Degerö, the REA system dynamically sampled reference gas using 2 s simulated wind signal to acquire identical up- and downdraft samples with respect to volume and GEM concentration. Accordingly, concentration bias between the REA sampling lines was corrected for in the GEM flux calculation.

2.4 Data processing

The analyzed air samples (Aa) for each cartridge were corrected for temperature sensitivity of the Hg detector by dividing the average GEM reference gas concentration over the entire campaign ($\overline{\mathrm{Ab_r}}$) through single GEM reference gas measurements ($\mathrm{Ab_r}$) according to

$$A_{\mathrm{corr}} = \mathrm{Aa} \cdot \frac{\overline{\mathrm{Ab_r}}}{\mathrm{Ab_r}}. \quad (5)$$

GEM concentrations ($\overline{C_{\mathrm{GEM}}}$) in up- and downdraft were computed by applying intercept (b) and slopes (s) calculated from the manual calibration procedure (Sect. 2.3.1) and the air volumes (V) drawn over the cartridges:

$$\overline{C_{\mathrm{GEM}}} = \frac{A_{\mathrm{corr}} - b}{s} \cdot \frac{1}{V}. \quad (6)$$

GEM concentration differences were corrected for the bias between the two sampling lines (Sect. 2.3.3). Finally, the

GEM flux was derived following Eq. (1). As the sampled air was not dried before being measured with a MFC calibrated for dry air, GEM fluxes were corrected for variations in the water vapor content of the air following Lee (2000):

$$F_{\mathrm{GEMcorr}} = (1 + 1.85\zeta)F_{\mathrm{GEM}} + 1.85\frac{\overline{\rho}_{\mathrm{GEM}}}{\overline{\rho}_{\mathrm{a}}}\mathrm{LE}_m, \quad (7)$$

where F_{GEMcorr} is the corrected and F_{GEM} the uncorrected GEM flux (ng m^{-2} h^{-1}). ζ is the water vapor mixing ratio (kg kg^{-1}). LE_m is the water vapor flux (ng m^{-2} h^{-1}), and the ratio of mean GEM density ($\overline{\rho}_{\mathrm{GEM}}$) to mean air density ($\overline{\rho}_{\mathrm{a}}$) were determined from the data for each measurement interval.

Criteria to identify conditions under which REA is not valid will be presented in Sect. 3.1.4. Among them an integral turbulent characteristics test was applied to identify the development of turbulent conditions:

$$\frac{\sigma_{\mathrm{w}}}{u_*} = 1.3 \cdot (1 - 2 \cdot \frac{z}{L})^{\frac{1}{3}}, \quad (8)$$

including σ_{w}, friction velocity (u_*), measuring height (z) and Obukhov length (L). Therein, the dependent integral turbulence characteristic for vertical wind velocity (σ_{w}/u_*) equates with a model dependent on stability (z/L) (Panofsky and Dutton, 1984; Foken and Wichura, 1996; Foken, 2006). A deviation by more than a factor of 2 from the model was used as the threshold to reject periods of insufficient turbulence as well as periods of larger than expected turbulence (Fig. S2).

The effect of a potentially dampened GEM flux due to high- and low-frequency losses of the turbulent eddies has been derived by interpretation of turbulence spectra for both sites dependent on instrumental properties (lateral sensor separation), measuring height, wind speed and stability conditions (Sect. 3.3). The applied high-pass filter (Eqs. 3, 4) amplifies the attenuation by reducing random or systematic noise in the flux estimates caused by low-frequency bias in the turbulent time series. High-frequency attenuation might be caused by an electronic delay of the valve switching and sensor separation (Foken et al., 2012).

To predict the size of REA flux source areas during the campaigns the footprint model of Kormann and Meixner (2001) was applied in Basel and a Lagrangian stochastic forward model following Rannik et al. (2000) at Degerö. The footprint models were chosen in order to fit the specific requirements as defined by the source areas at each site. The actual source area was estimated for each half-hour period based on wind direction, wind speed, stability, surface roughness and sensor height.

2.5 Site descriptions

The climate in the city of Basel, Switzerland (47.56° N, 7.58° E; 264 m a.s.l.), is temperate with a mean annual temperature of +9.8 °C and 776 mm precipitation (MeteoSchweiz, 2016). The REA system was deployed on the flat roof of the University of Basel's Meteorology, Climatology and Remote Sensing Laboratory (MCR) 20 m above the ground. The REA sampling inlets were mounted on the top of the permanently installed tower at 39 m above ground level. The average building height around the tower is 17 m and the 90 % cumulative footprint mirrors dominant wind directions, which are W to NW (240–340°) and ESE (100–140°). Results from this site reflect the situation within the urban inertial sublayer (Lietzke and Vogt, 2013).

The second campaign was conducted at an Integrated Carbon Observatory System (ICOS) site in the center of a boreal peatland in Sweden (64.18° N, 19.55° E; 270 m a.s.l.) during snowmelt. The mixed acid mire system covers 6.5 km^2 and is located in the Kulbäcksliden Research Park of the Svartberget Long-Term Experimental Research (LTER) facility near the town of Vindeln, county of Västerbotten, Sweden. The site is part of the Swedish research infrastructure (funded by the Swedish Research Council). The snow cover normally reaches a depth up to 0.6 m and lasts for 6 months on average (Sagerfors et al., 2008). The average total Hg concentrations in the upper 40 cm of the peatland soil are 57.3± 6.0 ng g^{-1} (± SD) dry matter, which is a typical value for soils in northern Sweden (Shanley and Bishop, 2012; Åkerblom et al., 2013). The climate of the site is defined as humid cold temperate with mean annual precipitation and temperature of 523 mm and +1.2 °C, respectively (Alexandersson et al., 1991). A measurement height of 1.8 m above the surface was maintained by gradually decreasing of the instrumentation boom to account for snowmelt. Dominant wind direction during summer is NE and SE during winter. For a more detailed site description see Granberg et al. (2001) or Peichl et al. (2013).

3 Results and discussion

3.1 REA performance

3.1.1 Sampling accuracy

Compared to single-inlet REA designs, systems with separate inlets for up- and downdraft are less prone to measurement uncertainty due to unsynchronized conditional sampling (Baker et al., 1992) and high-frequency concentration fluctuations in the tube flow (Moravek et al., 2013). Zhu et al. (2015b) found that the calculation of concentration differences based on temporally intermittent GEM measurements (non-stationarity of atmospheric GEM concentrations) introduced the largest source of uncertainty in their single-inlet Hg^0-REA system. Accurate simultaneous sampling of GEM concentration using a two-inlet design is thus the major technical improvement of our system compared to most Hg-REA systems used to date, as summarized in Sommar

et al. (2013a). However, even though the dual-inlet avoids a major source of error, there are a number of other aspects of a Hg-REA system that need to work as well as possible to measure land–atmosphere GEM fluxes. One of these is the determination of the β value, which includes sonic temperature and sensible heat flux measurements (Sect. 3.1.2). It is estimated to introduce an uncertainty similar to Zhu et al. (2015b) of approximately 10 %. Uncertainty due to flux dampening of sampled low- and high-frequency concentration fluctuations is small and just relevant during specific stability and wind speed conditions depending on measurement height and quality of turbulence (Sect. 3.3). There are several other sources of error in the measurements such as (i) the possible bias in vertical wind velocity measurements, (ii) the precision of the switching of the fast-response valves, (iii) the sampled air volume, (iv) the peak integration and (v) the field calibration procedure (cf. Zhu et al., 2015b).

i. Vertical wind velocity is used for instantaneous valve control. Ammann (1999) ascribed the main error here to be the possibility for misalignment between the wind field and the sensor head due to a tilted sensor setup or wind distortion around the sensor. However, the application of a high-pass filter combined with a deadband was able to alleviate averaged vertical wind velocity bias from the wind signal.

ii. It is important to limit the electronic delay to switch the fast-response valves caused by the digital measurements system and signal processing. The effective response time to actuate the fast-response valves was determined to be 18 ms for the opening and 8 ms for the closing. The switching of the fast-response valves allowed a maximal resolution between updraft and downdraft samples of 5.2 Hz.

iii. A major challenge in applying a system with two inlet tubes and no dry Hg-free air addition at the inlets (as applied by Sommar et al., 2013a) is to control flow pressure that builds up within the sampling lines. Flow surges are dependent on the time the fast-response valves remain closed. Pressure variations were dampened by a reservoir of 200 mL volume between the pump and mass flow controller (Fig. 1). The resistance within the lines was initially checked to be equal to minimize pressure anomalies between the three flow paths. A simulated wind signal with fast-response valve opening times of 2 s for the up- and downdraft and 1 s for the deadband was applied and revealed maximal pressure fluctuations of 35 mbar. The vast majority of the 30 min measurements in Basel and Degerö showed higher switching rates which are generally associated with lower pressure fluctuations. The total volumes drawn over updraft, downdraft and deadband lines averaged 30 ± 0.09 in Basel and 45 ± 0.01 L ($\pm$ SD) at Degerö. The proportion of the air not analyzed accounted for 10.5 L in Basel and 20.3 L at Degerö. Measurements were discarded if the volume deviated more than 2.5 % from the flow setting value of the mass flow controller (cf. Sect. 3.1.4).

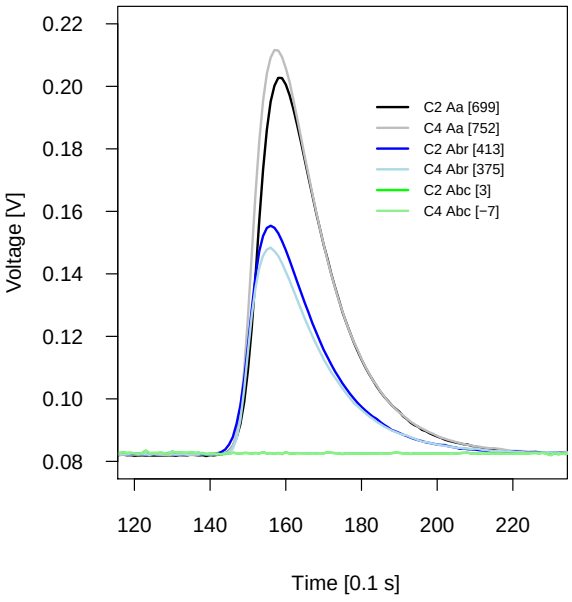

Figure 3. Representative peak recovery for gold cartridge pair C2–C4 during ambient air (Aa), GEM reference gas (Abr) and dry, Hg-free air measurements (Abc) on 11 February 2012, between 14:00 and 15:30 in Basel. The values in squared brackets equal the areas between the curves and the baseline. The plots show an extract of 10 s from the peak delay sequence which takes 30 seconds in total. *Y* axis indicates the Hg detector baseline voltage (V).

iv. An analysis of the detector peaks indicated that the signal for atmospheric and GEM reference gas samples were statistically different from blank measurements (99 % confidence) (Fig. 3).

v. The manual calibration procedure revealed a strong linear relationship between peak areas and syringe-injected GEM reference gas for the cartridge pairs (Fig. S1). The automated injection of GEM reference gas provided a 2-hourly quality control measure to monitor any bias caused by the temperature sensitivity of the Hg detector. The air temperature surrounding the Hg detector showed a strong linear relationship with the GEM reference gas measurements for up- and downdraft in Basel and a less pronounced dependence at Degerö (Fig. 4). The uncertainty of concentration measurements for our REA system is basically introduced by sampling-line bias, wherefrom the method detection limit is derived (Sects. 2.3.3 and 3.1.3).

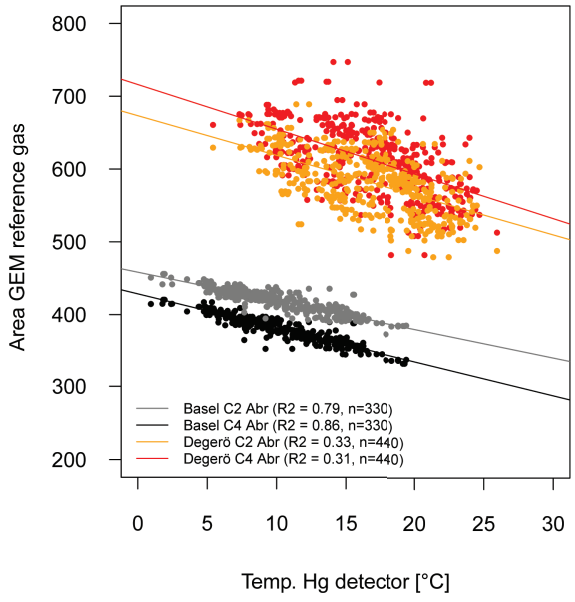

Figure 4. Linear relationship between GEM reference gas (Abr) measured with gold cartridge pair C2–C4 in Basel (grey, black) and Degerö (orange, red) and air temperatures within the Hg detector box.

3.1.2 β-factor evaluation

In this study, β is derived from EC time series of temperature and vertical wind speed at both sites (Eq. 2) during methodologically favorable conditions (cf. Sect. 3.1.4) with respect to turbulence for every 30 min GEM flux measurement averaging period. Due to considerable scatter in β especially during periods when sensible heat flux diminished to near zero, data were omitted for kinematic heat flux within the range of $\pm 0.01\,\mathrm{K\,m\,s^{-1}}$ (Ammann and Meixner, 2002; Sommar et al., 2013a). In accordance with Hensen et al. (2009) only β factors in the range of 0.1–1 were used. During the first study in Basel a fixed deadband of $|w| < 0.2\,\mathrm{m\,s^{-1}}$ was applied. This was done to restrict the analysis to periods when the discrimination between updraft and downdraft was large enough to allow for accurate estimation and to prolong the opening times of the fast-response valves. At Degerö a dynamic deadband approach with a sampling threshold $\pm 0.5\sigma_w$ was used. Data analysis revealed that the effect of surface layer stability or u_* on β calculation was negligible. The median $\pm$ mad (median absolute deviation) of observed β values in Basel and Degerö was 0.49 ± 0.21 ($n = 391$) and 0.45 ± 0.20 ($n = 342$), respectively. Median β values observed at Basel and Degerö concurred with literature in the range of 0.4–0.6 (Grönholm et al., 2008; Bash and Miller, 2009; Arnts et al., 2013; Sommar et al., 2013a).

The Basel measurements resulted in broad non-Gaussian frequency distributions for the fraction of time when air was sampled into up- and down reservoirs. The average cumulated opening times for the 30 min sampling periods for the up- and downdrafts were 9.6 and 9.8 min, respectively, which results in maxima in up/down/deadband sampling fractions of about 32/33/35 %. Periods of less developed turbulence caused the fast-response valves to switch less often and increased the opening times of the deadband. The corresponding confined frequency distributions observed at Degerö were 28/27/45 % and showed significantly lower variation than for the Basel measurements.

3.1.3 Detection limit

The instrument detection limit of the Hg detector was $< 0.1\,\mathrm{ng\,m^{-3}}$ and allowed discernment of GEM peaks from the baseline noise for all measurements. The gold cartridge pair offset criteria and the method detection limit were derived in the field from sampling the same air through updraft and downdraft lines. For this study we defined two strict rejection criteria for (1) maximum standard deviation of the offset of 0.05 and (2) maximum difference in gold cartridge response of 10 %. The assessment of the offset between the sampling lines during the Basel measurements was 0.009 ± 0.06 ($\pm$ SD) and $0.016 \pm 0.01\,\mathrm{ng\,m^{-3}}$ for gold cartridge pairs 1–3 and 2–4, respectively. At Degerö the offset was 0.17 ± 0.06 and $-0.004 \pm 0.02\,\mathrm{ng\,m^{-3}}$ for 1–3 and 2–4. If up- and downdraft lines sample the same air, the offset between these should be constant, independent of air Hg content. Scaling the GEM area difference detected in the up- and downdraft air by GEM area of the updraft air revealed an erroneous behavior of cartridge pair 1–3. Further inspection showed that the PTFE valves (V4–V7) seemed to restrict the air flow when energized, thus leading to erroneous air volume readings. In contrast, when air flows through cartridge pair 2–4, the valves are in the idle mode with free flow. Therefore, measurements with cartridge pair 1–3 were discarded for both campaigns due to the above threshold variability in Basel and the large gold cartridge pair offset at Degerö. Although data availability was reduced by 50 % this technical shortcoming may be solved by use of different valves, e.g., three-way flipper valves. Detailed results from the sampling line bias tests are presented in Figs. S3 and S4.

From these individual sampling lines bias measurements for Basel and Degerö a minimum detectable GEM concentration difference based on 1σ was derived. Thus, 98 % of the available 30 min data in Basel and 83 % at Degerö were above that limit. Zhu et al. (2015b) reported that 55 % of their Hg-REA flux data were significantly different from zero. Data from bias determination for cartridge pair 2–4 did not reveal any significant diurnal pattern or trend over time for both sites.

3.1.4 Data coverage

Based on the systematic bias when using cartridge pair 1–3, 50 % of the data from both sites, Basel and Degerö were discarded (Table 1). Some of the remaining flux measure-

Table 1. Overview of rejection criteria for the evaluation of REA field measurements. Rejected amount of data (%) and remaining numbers of observations (n) are given.

Criterion	Rejection percentage	
	Basel	Degerö
Gold cartridge pair offset	50 %	50 %
Logging failure	4 %	7 %
Insufficient turbulence (σ_w/u_*)	6 %	4 %
Extreme stability ($\lvert z/L\rvert > 2$)	0 %	0 %
Sampling air flow and blank irregularities	1 %	4 %
Total rejection (excl. cartridge pair offset)	12 %	16 %
Remaining observations	$n = 292$	$n = 380$

ments were rejected due to logging failures including power breakdowns. Additionally, 6 % of the data at Basel and 4 % at Degerö were rejected due to poorly developed turbulence, determined by applying an integral turbulent characteristics test (Eq. 8). GEM flux measurements during extremely stable conditions were omitted ($z/L > 2$). The data were also screened for irregularities in the measured sampling air flow (deviation from the flow setting value > 2.5 %). Dry Hg-free air was used to determine possible cartridge or sampling line contamination and to discard periods of a noisy Hg detector baseline, due to rapid temperature changes within the detector box. GEM flux measurements were discarded when the signal of the blank measurements exceeded 10 % of the integration peak area that was detected for atmospheric GEM. In other Hg-REA studies, 44 % (Sommar et al., 2013a) and 28 % (Zhu et al., 2015b) of the data were flagged as moderate and low data quality due to turbulence characteristics (cf. Mauder and Foken, 2004). In our study the overall half-hourly data loss was 62 % at Basel and 66 % at Degerö.

3.2 Meteorological conditions

During the measurements in Basel air temperatures averaged -7.9 ± 3.3 °C ($\pm$ SD). Precipitation occurred in the first 2 days and caused substantial loss of EC data, while GEM flux determination was not affected. From 3 to 12 February 2012, measurements were done during predominantly cloudless conditions with daily solar radiation (Rg) peaks between 300 and 500 W m^{-2}. Relative humidity ranged between 20 and 91 % and was on average significantly lower in Basel than at Degerö. Wind speed in Basel averaged 2.6 m s^{-1} and did not differ significantly between day (Rg > 5 W m^{-2}) and night (Rg < 5 W m^{-2}). Wind direction was predominantly from the northwest during the day and the southeast during the night. Polar histograms of 30 min averaged wind speed and atmospheric GEM concentration measurements at both sites are presented in Fig. S5. Unstable atmospheric stratification ($z/L < -0.05$) was predominant (92 % of time) during the Basel campaign while less than 3 % of the measurements were conducted during stable conditions ($z/L > 0.05$).

The campaign on the boreal peatland commenced on 5 May 2012. The surface was covered by maximum of 33 cm snow which melted away towards the end of the campaign on 24 May 2012. A total precipitation amount of 19.6 mm was recorded during the campaign including a heavy snowfall during the morning of 6 May. Air temperatures averaged 5.4 ± 3.5 °C, whereas daily averages increased from 0.0 to 9.1 °C over the period. Soil temperatures at 2 cm depth likewise increased from 3.2 to 8.0 °C (daily averages). The prevailing wind direction at Degerö was from the northeast to south with an average wind speed at 2.9 m s^{-1} (daytime mean: 3.1 m s^{-1}, nighttime mean: 2.1 m s^{-1}). Conditions were stable ($z/L > 0.02$) 22 % of the time (daytime: 15 %, nighttime: 43 %), unstable for another 38 % (daytime: 42 %, nighttime: 22 %) ($z/L < -0.02$) and neutral during the remaining 40 % (daytime: 43 %, nighttime: 35 %).

3.3 Footprint and turbulence regime

In Basel the GEM flux measurements were conducted over a rough surface showing strongly modified vertical turbulent exchange processes. Measurements were conducted within the inertial sublayer 39 m above ground, which overlays the urban roughness sublayer assuming that the upper level of the roughness sublayer is about 2 times the average building height of 17 m (Feigenwinter et al., 2012). Of the GEM fluxes measured in Basel, 90 % originated from a source area that covered 78 ha and reflected a blended, spatially averaged signal (Fig. 5a). Within that footprint the water fraction accounts for 7 %, the vegetation fraction for 19 %, the building fraction for 36 % and impervious ground surface for 38 %. Main wind directions during the campaign mimicked the dominant seasonal wind direction from NNW and ESE.

An inspection of the normalized co-spectra for sensible heat, latent heat and CO_2 flux revealed the occurrence of large eddies leading to comparably low switching intervals of 1.4 ± 0.3 Hz (mean $\pm$ SD). The co-spectral estimates were derived from 20 Hz data over the entire campaign during unstable conditions and demonstrate that high-frequency losses for sensible heat, latent heat and CO_2 fluxes were minimal. Low-frequency losses resulted due to the applied high-pass filter which attenuated fluctuations at periods larger than the time constant of 16.6 min (RF in Fig. 6). Ogives were calculated after Foken et al. (2012) and converged at approximately 90 % of all cases within the 30 min averaging period (Fig. 6a). Simulated damping factors for REA fluxes revealed that at a mean wind speed of 2.6 m s^{-1} less than 10 % of the flux was dampened. We conclude that applying a 30 min averaging interval, a high-pass filter and valve switching at 10 Hz was adequate for REA flux calculations since considerable flux damping occurred just at low-frequency ranges, unstable conditions and low wind velocities.

At Degerö, 90 % of the footprint comprised 0.6 ha (Fig. 5b). For all contour lines calculated, the surface was physically homogenous. The roughness length z_0 present

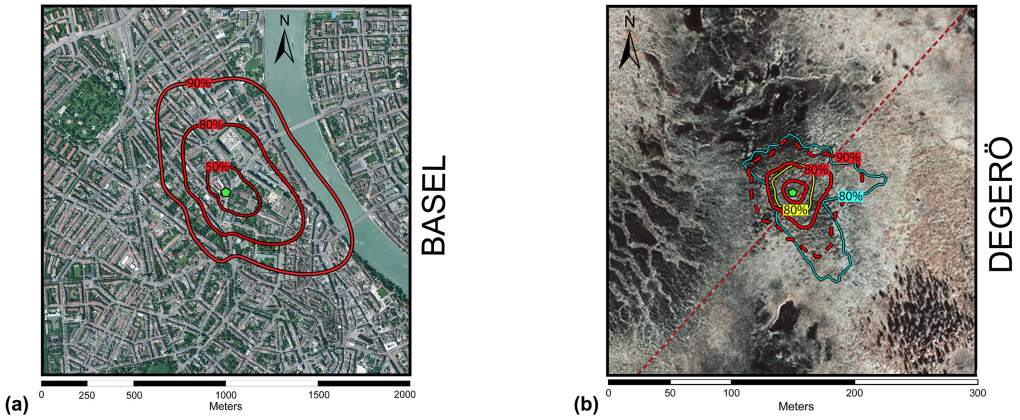

Figure 5. Aerial RGB and IR photographs with red contours containing 50, 80 and 90 % of the flux during the campaign in Basel **(a)** and Degerö **(b)**. The yellow and blue 80 % contours at Degerö stand for unstable and stable conditions, respectively. The light-green pentagons indicate the location of the flux towers.

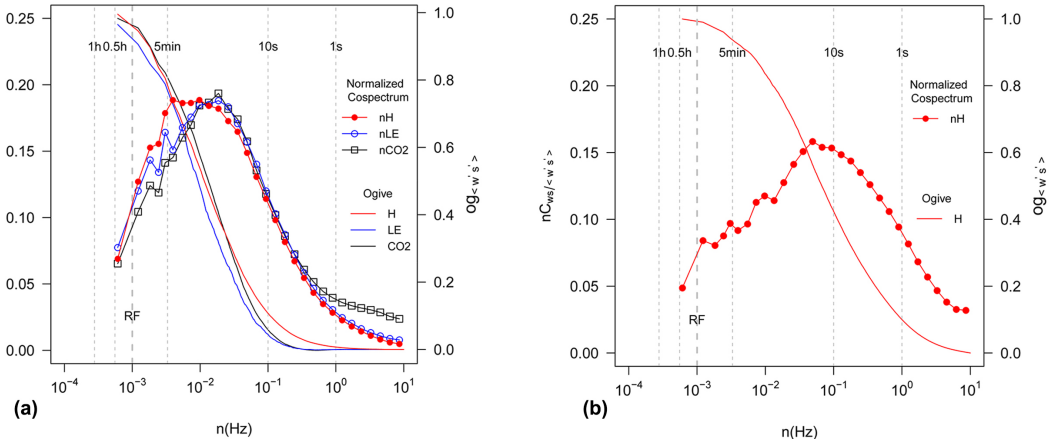

Figure 6. Normalized turbulence co-spectra (y axis, lines + symbols) and converging ogives (secondary y axis, lines) of sensible heat (red), latent heat (blue) and CO_2 flux (black) during unstable conditions for Basel **(a)** and Degerö **(b)**. The vertical line labeled as RF indicates the time constant of the applied high-pass filter. At Degerö only high-resolution air temperature data were used.

during the campaign was only a few millimeters due to the short vegetation (Sagerfors et al., 2008) and negligible when there was snow cover. During the Degerö campaign, the normalized turbulence spectra and ogives were derived for sensible heat flux during unstable conditions (Fig. 6b). Due to temporary technical problems regarding the LI-6262 closed-path infrared gas analyzer, CO_2 and latent heat flux data were not used for spectral analysis. In comparison to Basel the co-spectrum of the sensible heat flux was shifted significantly towards higher frequencies. The occurrence of more smaller eddies increased the fast-response valve switching interval (2.9 ± 0.7 Hz; mean $\pm$ SD) which increased with increasing u_* (Fig. S6). High-frequency losses at 10 Hz accounted for less than 5 % of the sensible heat flux. The ogive converged a constant value at RF and indicates that large eddies were sampled completely over the averaging period (Fig. 6b). At Degerö the integral damping factor for the REA flux was more than 20 % at high frequencies especially during stable and strong wind conditions. Simulated integral REA flux damping factors dependent on wind speed and stability conditions and cospectral density plots for site-averaged wind speeds are illustrated for Basel and Degerö in Figs. S7 and S8.

3.4 Atmospheric GEM concentrations

Mean $\pm$ SD atmospheric GEM concentration in Basel was $4.1 \pm 1\,\mathrm{ng\,m^{-3}}$. The average concentration difference between up and downdraft was $0.26 \pm 0.3\,\mathrm{ng\,m^{-3}}$ (median: $0.19\,\mathrm{ng\,m^{-3}}$) (Fig. 7). It might be possible that during the exceptionally cold period in Basel gas and oil-fired thermal power stations within the dense urban source area contributed to enhanced atmospheric GEM concentrations. In urban areas, total gaseous Hg concentrations were highest during heating season (Fang et al., 2004). Highest GEM lev-

Table 2. Summary of averaged, median and distribution of GEM fluxes, atmospheric GEM concentrations and environmental conditions during the measurement campaigns. Pearson correlation coefficients (r) between GEM flux and environmental parameters are given when statistically significant ($p < 0.05$).

Variable		Basel				Degerö			
	Unit	Mean	Median	10th/90th percentile	r	Mean	Median	10th/90th percentile	r
GEM flux	$ng\,m^{-2}\,h^{-1}$	15.4	34.9	−262/270	–	3.0	2.6	−71/67	–
GEM concentration	$ng\,m^{-3}$	4.1	3.9	3.3/5.6	−0.23	1.6	1.6	1.4/1.8	−0.14
Sensible heat flux (EC)	$W\,m^{-2}$	73.5	65	20/134	–	11.8	2.4	−17/58	0.23
Latent heat flux (EC)	$W\,m^{-2}$	12.3	10.6	1.8/24.5	0.26	–	–	–	–
CO_2 flux (EC)	$\mu mol\,m^{-2}\,s^{-1}$	0.02	0.01	0/0.04	0.36	–	–	–	–
Friction velocity	$m\,s^{-1}$	0.41	0.39	0.2/0.7	0.2	0.19	0.18	0.07/0.34	−0.23
Wind speed	$m\,s^{-1}$	2.6	2.5	1.3/3.9	0.13	2.9	2.7	1.0/4.8	−0.26
Solar radiation	$W\,m^{-2}$	78	–	0/312	−0.22	159	–	0/455	0.14
Air temperature	°C	−7.9	−8	−12/3.4	0.23	5.3	5.4	0.1/10.2	0.26
Soil temperature	°C	–	–	–	–	6.7	7	4.4/8.2	0.2
Relative humidity	%	62	60	40/85	−0.23	76	80	47/98	−0.3

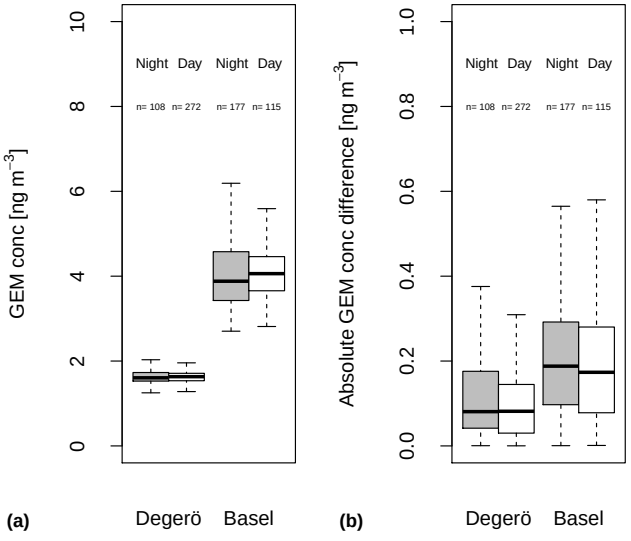

Figure 7. Box plots display atmospheric GEM concentrations **(a)** and the absolute GEM concentration differences between updraft and downdraft **(b)** during the day and night at Degerö and Basel.. Number of observations is indicated. The bold line in the box represents the median GEM concentration. The horizontal border lines indicate the 25th (Q1) and 75th (Q3) percentiles, from bottom to top. The lower whisker marks Q1 minus 1.5 times the interquartile range (IQR). The upper whisker marks Q3 plus 1.5 IQR. Outliers are not displayed.

els in Basel were observed during periods of low wind velocities ($u_* < 0.3\,m\,s^{-1}$) and southern wind directions. Most likely additional GEM emissions from vehicular traffic along a highly frequented road contributed to elevated Hg concentrations during southerlies. GEM concentrations in the exhaust of motor vehicles in driving mode are elevated and range from 2.8 to 26.9 $ng\,m^{-3}$ depending on fuel types (Won et al., 2007). The road runs in a north/south direction and is the major source of CO_2 (Lietzke and Vogt, 2013).

The average air concentration during snowmelt at Degerö was $1.6 \pm 0.2\,ng\,m^{-3}$, comparable to observations made in 2009 by static chambers (Fritsche et al., 2014). Concentration difference in REA conditional samples collected at Degerö averaged $0.13 \pm 0.2\,ng\,m^{-3}$ (median: $0.09\,ng\,m^{-2}$) which is about a factor of 2 lower than the magnitude observed in Basel (Fig. 7). No significant concentration relationships were found with either wind direction or atmospheric stability.

3.5 GEM flux estimation in contrasting environments

Urban areas are of particular concern with respect to the global Hg cycle. Industrial sectors and anthropogenic combustion processes emit large quantities of Hg to the atmosphere (Walcek et al., 2003) where mostly gaseous oxidized Hg and particulate bound Hg deposit locally. Highly variable Hg air concentrations, the physically and chemically diverse nature of urban surface covers and urban meteorology (e.g., heat island effect) are suggested to create complex Hg flux patterns above cities (Gabriel et al., 2005). Up to now, just a handful of studies have described GEM emissions from urban environments (Kim and Kim, 1999; Feng et al., 2005; Gabriel et al., 2006; Obrist et al., 2006; Eckley and Branfireun, 2008). GEM fluxes measured in Basel showed a diurnal trend with a maximum deposition around noon and highest emissions around 7 PM (Fig. 8a). The mean flux ± SE of $15.4 \pm 13.3\,ng\,m^{-2}\,h^{-1}$ indicated that this urban area was a net source of atmospheric Hg during the study period. Similarly, for the same site in spring and fall, Obrist et al. (2006) observed average GEM emissions of $6.5 \pm 0.9\,ng\,m^{-2}\,h^{-1}$ (± SD) in the stable nocturnal boundary layer using the $^{222}Rn/Hg^0$ method. Environmental variables, e.g., solar radiation, air and soil temperatures, are known to be major drivers of natural GEM emission (e.g., Schröder et

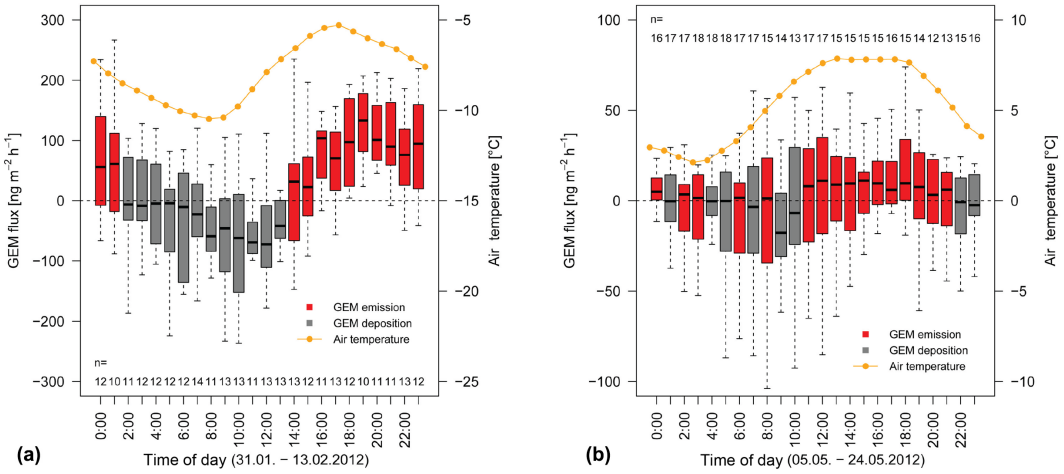

Figure 8. Diurnal patterns of GEM flux during the campaign in Basel **(a)** and Degerö **(b)** using the 6-hourly smoothed GEM flux time series. Red and gray colored box plots indicate median Hg emission and Hg deposition at different times of the day, respectively. Hourly averages of air temperatures are given (orange). Horizontal dashed line indicates the zero line of GEM flux and/or air temperature. Box plot description in caption of Fig. 7.

al., 1989; Steffen et al., 2002; Choi and Holsen, 2009). Correlations between GEM flux and its controlling factors for this study can be reviewed in Table 2. Northwesterly wind directions were associated with GEM deposition between 02:00 and 13:00. In contrast, emission events were linked to wind directions from the southeast.

Determination of GEM snow–air exchange has been a subject of interest since the first atmospheric mercury depletion events were observed (Schröder et al., 1998). Non-arctic GEM flux studies from snowpack report deposition as well as emission events with near zero net fluxes (Faïn et al., 2007; mean: $0.4\,\mathrm{ng\,m^{-2}\,h^{-1}}$; Fritsche et al., 2008b; mean: $0.3\,\mathrm{ng\,m^{-2}\,h^{-1}}$).

The mean GEM snow–air transfer observed at Degerö was $3.0 \pm 3.8\,\mathrm{ng\,m^{-2}\,h^{-1}}$ ($\pm$ SE). It is the result of a balance between deposition prevailing from midnight to noon and vice versa during the rest of the day when emission predominates (Fig. 8b). REA fluxes varied strongly during both the day and night but revealed a significant difference between GEM fluxes during unstable (median: $8.7\,\mathrm{ng\,m^{-2}\,h^{-1}}$), stable (median: $-0.1\,\mathrm{ng\,m^{-2}\,h^{-1}}$) and neutral conditions (median: $-4\,\mathrm{ng\,m^{-2}\,h^{-1}}$) (Mann–Whitney U test, $p < 0.05$). GEM concentrations in the surface snow layers were not determined in this study but in accordance with Faïn et al. (2013), GEM is likely enhanced during the course of daytime compared to ambient air due to sunlight-mediated processes. An impact of fresh snowfall and possible wet Hg deposition on GEM fluxes could not be observed with REA but precipitation events occurred regularly in the afternoon and might have contributed to GEM volatilized in the evenings together with GEM produced during dusk and night (Faïn et al., 2013).

GEM flux quantification is improved, compared to previous systems, by the synchronous sampling, as well the regular monitoring of GEM reference gas concentration and dry, Hg-free air. As demonstrated here, these improvements make REA feasible for measurements over tall buildings but also short vegetation and snow cover. At Degerö, however, higher abundance of smaller eddies increased the GEM flux variability. However, the REA technique remains better suited to assessing magnitudes and variability of fluxes rather determining the effects of short-term variability in environmental parameters on GEM fluxes (cf. Gustin et al., 1999).

For future long-term REA applications we have three suggestions: (i) a more regular determination of the bias between both sampling lines, either by a weekly check of the bias or by implementing an additional valve to switch up- and downdraft lines every hour (each cartridge would measure up- and downdraft); (ii) although Hg detector sensitivity due to rapid air temperature changes is corrected for, it could be avoided to a large extent by using a more effective temperature control unit; (iii) improvement of the accuracy in the air volumes sampled by installing mass flow meters for up- and downdraft lines.

4 Conclusions

The need to precisely determine GEM land–atmosphere exchange over long continuous periods is widely recognized. REA has the potential to do this more effectively than other methods. Therefore, several REA systems have been deployed, but their accuracy has been impaired by several design features such as the use of multiple detectors and nonsynchronous sample collection. We developed a dual-inlet, single analyzer system that has overcome these shortcom-

ings and included new features such as the integrated GEM reference gas and Hg zero-air generator for continuous monitoring of GEM recovery, as well as blank measurements. The data acquisition and control system is fully automated and could be remotely controlled, which reduces the workload compared to other REA systems. We have demonstrated the system in contrasting environments to measure turbulent transport of GEM 39 m above ground level in Basel, Switzerland, and 1.8 m above a boreal peatland in Sweden during snowmelt. While the demonstration identified room for further improvements, we believe this novel design has the potential to facilitate the use of REA for measuring land–atmosphere Hg exchange for sustained periods in a variety of environments.

The Supplement related to this article is available online at doi:10.5194/amt-9-509-2016-supplement.

Acknowledgements. This research was funded by the Swedish Research Council (2009-15586-68819-37), the Department of Earth Sciences, Uppsala University, and the Department of Environmental Geosciences, University of Basel. We thank William Larsson and the late Lars Lundmark from Umeå University for technical assistance and engineering and Roland Vogt from the University of Basel's MCR lab for using the EC setup. The study at Degerö also received technical and maintenance support from the Svartberget Experimental Forest, Vindeln, Sweden. The study was also supported by the Swedish research infrastructures, ICOS Sweden (Integrated Carbon Observatory System) and SITES (Swedish Infrastructure for Ecosystem Science) at Degerö, both partly financed by the Swedish Research Council.

Edited by: M. Hamilton

References

Agnan, Y., Le Dantec, T., Moore, C. W., Edwards, G. C., and Obrist, D.: New constraints on terrestrial surface-atmosphere fluxes of gaseous elemental mercury using a global database, Environ. Sci. Technol., 50, 507–524, 2016.

Åkerblom, S., Bishop, K., Bjorn, E., Lambertsson, L., Eriksson, T., and Nilsson, M. B.: Significant interaction effects from sulfate deposition and climate on sulfur concentrations constitute major controls on methylmercury production in peatlands, Geochim. Cosmochim. Ac., 102, 1–11, 2013.

Alexandersson, H., Karlström, C., and Larsson-McCann, S.: Temperaturen och nederbörden i Sverige 1961–1990, The Swedish Meteorological and Hydrological Institute, Norrköping, Sweden, 1991.

Ammann, C.: On the applicability of Relaxed Eddy Accumulation and Common Methods for Measuring Trace Gas Fluxes, PhD Thesis, ETH Zürich, Zürich, 229 pp., 1999.

Ammann, C. and Meixner, F. X.: Stability dependence of the relaxed eddy accumulation coefficient for various scalar quantities, J. Geophys. Res., 107, 4071, doi:10.1029/2001JD000649, 2002.

Arnts, R. R., Mowry, F. L., and Hampton, G. A.: A high-frequency response relaxed eddy accumulation flux measurement system for sampling short-lived biogenic volatile organic compounds, J. Geophys. Res.-Atmos., 118, 4860–4873, 2013.

Baker, J. M., Norman, and Bland, W. L.: Field-scale application of flux measurement by conditional sampling, Agric. Forest Meteorol., 62, 31–52, 1992.

Bash, J. O. and Miller, D. R.: A note on elevated total gaseous mercury concentrations downwind from an agriculture field during tilling, Sci. Total Environ., 388, 379–388, 2007.

Bash, J. O. and Miller, D. R.: A relaxed eddy accumulation system for measuring surface fluxes of total gaseous mercury, J. Atmos. Ocean. Tech., 25, 244–257, 2008.

Bash, J. O. and Miller, D. R.: Growing season total gaseous mercury (TGM) flux measurements over an *Acer rubrum* L. stand, Atmos. Environ., 43, 5953–5961, 2009.

Bauer, D., Campuzano-Jost, P., and Hynes, A. J.: Rapid, ultrasensitive detection of gas phase elemental mercury under atmospheric conditions using sequential two-photon laser induced fluorescence, J. Environ. Monitor., 4, 339–343, 2002.

Brut, A., Legain, D., Durand, P., and Laville, P.: A relaxed eddy accumulator for surface flux measurements on ground-based platforms and aboard research vessels, J. Atmos. Ocean. Tech., 21, 411–427, 2004.

Businger, J. and Oncley, S.: Flux Measurement with Conditional Sampling, J. Atmos. Ocean. Tech., 7, 349–352, 1990.

Choi, H.-D. and Holsen, T. M.: Gaseous mercury fluxes from the forest floor of the Adirondacks, Environ. Pollut., 157, 592–600, 2009.

Cobos, D. R., Baker, J. M., and Nater, E. A.: Conditional sampling for measuring mercury vapor fluxes, Atmos. Environ., 36, 4309–4321, 2002.

Converse, A. D., Riscassi, A. L., and Scanlon, T. M.: Seasonal variability in gaseous mercury fluxes measured in a high-elevation meadow, Atmos. Environ., 44, 2176–2185, 2010.

Desjardins, R. L.: Energy budget by an eddy correlation method, J. Appl. Meteorol., 16, 248–250, 1977.

Eckley, C. S. and Branfireun, B.: Gaseous mercury emissions from urban surfaces: controls and spatiotemporal trends, Appl. Geochem., 23, 369–383, 2008.

Eckley, C. S., Gustin, M., Lin, C.-J., Li, X., and Miller, M. B.: The influence of dynamic chamber design and operating parameters on calculated surface-to-air mercury fluxes, Atmos. Environ. 44, 194–203, 2010.

Faïn, X., Grangeon, S., Bahlmann, E., Fritsche, J., Obrist, D., Dommergue, A., Ferrari, C. P., Cairns, W., Ebinghaus, R., Barbante, C., Cescon, P., and Boutron, C.: Diurnal production of gaseous mercury in the alpine snowpack before snowmelt, J. Geophys. Res., 112, D21311, doi:10.1029/2007JD008520, 2007.

Faïn, X., Moosmüller, H., and Obrist, D.: Toward real-time measurement of atmospheric mercury concentrations using cavity ring-down spectroscopy, Atmos. Chem. Phys., 10, 2879–2892, doi:10.5194/acp-10-2879-2010, 2010.

Faïn, X., Helmig, D., Hueber, J., Obrist, D., and Williams, M. W.: Mercury dynamics in the Rocky Mountain, Colorado, snowpack,

Biogeosciences, 10, 3793–3807, doi:10.5194/bg-10-3793-2013, 2013.

Fang, F., Wang, Q., and Li, J.: Urban environmental mercury in Changchun, a metropolitan city in Northeastern China: source, cycle, and fate, Sci. Total Environ., 330, 159–170, 2004.

Feigenwinter, C., Vogt, R., and Christen, A.: Eddy covariance measurements over urban areas, in: Eddy Covariance – a Practical Guide to Measurement and Data Analysis, edited by: Aubinet, M., Vesala, T., and Papale, D., Springer Science + Business Media B.V., Dordrecht, the Netherlands, 377–397, 2012.

Feng, X. B., Wang, S. F., Qiu, G. A., Hou, Y. M., and Tang, S. L.: Total gaseous mercury emissions from soil in Guiyang, Guizhou, China, J. Geophys. Res.-Atmos., 110, D14306, doi:10.1029/2004JD005643, 2005.

Foken, T.: Angewandte Meteorologie, Mikrometeorologische Methoden, 2. Auflage, Springer, Berlin, 2006.

Foken, T. and Wichura, B.: Tools for quality assessment of surface-based flux measurements, Agr. Forest Meteorol., 78, 83–105, 1996.

Foken, T., Leuning, R., Oncley, S. R., Mauder, M., and Aubinet., M.: Corrections and data quality control, in: Eddy Covariance – a Practical Guide to Measurement and Data Analysis, edited by: Aubinet, M., Vesala, T., and Papale, D., Springer Science + Business Media B.V., Dordrecht, the Netherlands, 85–131, 2012.

Fritsche, J., Obrist, D., Zeeman, M. J., Conen, F., Eugster, W., and Alewell, C.: Elemental mercury fluxes over a sub-alpine grassland determined with two micrometeorological methods, Atmos. Environ., 42, 2922–2933, 2008a.

Fritsche, J., Wohlfahrt, G., Ammann, C., Zeeman, M., Hammerle, A., Obrist, D., and Alewell, C.: Summertime elemental mercury exchange of temperate grasslands on an ecosystem-scale, Atmos. Chem. Phys., 8, 7709-7722, doi:10.5194/acp-8-7709-2008, 2008b.

Fritsche, J., Osterwalder, S., Nilsson, M. B., Sagerfors, J., Åkerblom, S., Bishop., K., and Nilsson., M.: Evasion of elemental mercury from a boreal peatland suppressed by long-term sulfate addition, Environ. Sci. Technol., 1, 421–425, 2014.

Gabriel, M. C., Williamson, D., Lindberg, S., Zhang, H., and Brooks, S.: Spatial variability of total gaseous mercury emission from soils in a southeastern US urban environment, Environ. Geol., 48, 955–964, 2005.

Gabriel, M. C., Williamson, D. G., Zhang, H., Brooks, S., and Lindberg, S.: Diurnal and seasonal trends in total gaseous mercury flux from three urban ground surfaces, Atmos. Environ., 40, 4269–4284, 2006.

Gaman, A., Rannik, Ü., Aalto, P., Pohja, T., Siivola, E., Kulmala, M., and Vesala, T.: Relaxed eddy accumulation system for size-resolved aerosol particle flux measurements, J. Atmos. Ocean. Tech., 21, 933–943, 2004.

Gillis, A. and Miller, D. R.: Some potential errors in the measurement of mercury gas exchange at the soil surface using a dynamic flux chamber, Sci. Total Environ., 260, 181–189, 2000.

Granberg, G., Sundh, I., Svensson, B. H., and Nilsson, M.: Effects of temperature, and nitrogen and sulfur deposition, on methane emission from a boreal mire, Ecology, 82, 1982–1998, 2001.

Grigal, D. F.: Inputs and outputs of mercury from terrestrial watersheds: a review, Environ. Rev., 10, 1–39, 2002.

Grönholm, T., Haapanala, S., Launiainen, S., Rinne, J., Vesala, T., and Rannik, Ü.: The dependence of the beta coefficient of REA system with dynamic deadband on atmospheric conditions, Environ. Pollut., 152, 597–603, 2008.

Gustin, M. S.: Exchange of mercury between the atmosphere and terrestrial ecosystems, in: Advances in Environmental Chemistry, and Toxicology of Mercury, edited by: Cai, Y., Liu, G., and O'Driscoll, N. J., John Wiley & Sons, Hoboken, NJ, USA, 423–452, 2011.

Gustin, M. S. and Lindberg, S. E.: Terrestrial Hg fluxes: is the next exchange up, down, or neither?, in: Dynamics of Mercury Pollution on Regional and Global Scales, edited by: Pirrone, N. and Mahaffey, K. R., Springer, New York, 241–259, 2005.

Gustin, M. S., Lindberg, S., Marsik, F., Casimir, A., Ebinghaus, R., Edwards, G., Hubble-Fitzgerald, C., Kemp, R., Kock, H., Leonard, T., London, J., Majewski, M., Montecinos, C., Owens, J., Pilote, M., Poissant, L., Rasmussen, P., Schaedlich, F., Schneeberger, D., Schroeder, W., Sommar, J., Turner, R., Vette, A., Wallschlaeger, D., Xiao, Z., and Zhang, H.: Nevada STORMS project: measurement of mercury emissions from naturally enriched surfaces, J. Geophys. Res.-Atmos., 104, 21831–21844, 1999.

Gustin, M. S., Lindberg, S. E., Austin, K., Coolbaugh, M., Vette, A., and Zhang, H.: Assessing the contribution of natural sources to regional atmospheric mercury budgets, Sci. Total Environ., 259, 61–71, 2000.

Gustin, M. S., Lindberg, S. E., and Weisberg, P. J.: An update on the natural sources and sinks of atmospheric mercury, Appl. Geochem., 23, 482–493, 2008.

Haapanala, S., Rinne, J., Pystynen, K.-H., Hellén, H., Hakola, H., and Riutta, T.: Measurements of hydrocarbon emissions from a boreal fen using the REA technique, Biogeosciences, 3, 103–112, doi:10.5194/bg-3-103-2006, 2006.

Hensen, A., Nemitz, E., Flynn, M. J., Blatter, A., Jones, S. K., Sørensen, L. L., Hensen, B., Pryor, S. C., Jensen, B., Otjes, R. P., Cobussen, J., Loubet, B., Erisman, J. W., Gallagher, M. W., Neftel, A., and Sutton, M. A.: Inter-comparison of ammonia fluxes obtained using the Relaxed Eddy Accumulation technique, Biogeosciences, 6, 2575–2588, doi:10.5194/bg-6-2575-2009, 2009.

Keeler, G. J. and Landis, M. S.: Standard Operating Procedure for Sampling Vapor Phase Mercury, University of Michigan, USA, 1994.

Kim, K. H. and Kim, M. Y.: The exchange of gaseous mercury across soil–air interface in a residential area of Seoul, Korea, Atmos. Environ., 33, 3153–3165, 1999.

Kim, K.-H., Lindberg, S. E., and Meyers, T. P.: Micrometeorological measurements of mercury vapor fluxes over background forest soils in eastern Tennessee, Atmos. Environ., 29, 267–282, 1995.

Kormann, R. and Meixner, F. X.: An analytical footrpint model for non-neutral stratification, Bound.-Lay. Meteorol., 99, 207–224, 2001.

Lee, X. H.: Water vapor density effect on measurements of trace gas mixing ratio and flux with a massflow controller, J. Geophys. Res.-Atmos., 105, 17807–17810, 2000.

Lietzke, B. and Vogt, R.: Variability of CO_2 concentrations and fluxes in and above an urban street canyon, Atmos. Environ., 74, 60–72, 2013.

Lindberg, S. and Meyers, T.: Development of an automated micrometeorological method for measuring the emission of mercury vapor from wetland vegetation, Wetl. Ecol. Manag., 9, 333–347, 2001.

Lindberg, S., Bullock, R., Ebinghaus, R., Engstrom, D., Feng, X., Fitzgerald, W., Pirrone, N., and Seigneur, C.: A synthesis of progress and uncertainties in attributing the sources of mercury in deposition, Ambio, 36, 19–32, 2007.

Mason, R. P. and Sheu, G.-R.: Role of the ocean in the global mercury cycle, Global Biogeochem. Cy., 16, 1093, doi:10.1029/2001GB001440, 2002.

Mauder, M. and Foken, T.: Documentation and Instruction Manual of the Eddy Covariance Software Package TK2, vol. 26, Arbeitsergebnisse, Universitat Bayreuth, Abteilung Mikrometeorologie, Bayreuth, 42 pp., ISSN 1614–8916, 2004.

McMillen, R.: An Eddy-correlation technique with extended applicability to non-simple terrain, Bound.-Lay. Meteorol., 43, 231–245, 1988.

MeteoSchweiz: Klimanormwerte Basel/Binningen, Normperiode 1961–1990, available at: http://www.meteoschweiz.admin.ch, last access: 10 January, 2016.

Meyers, T. P., Hall, M. E., Lindberg, S. E., and Kim, K.: Use of the modified Bowen-ratio technique to measure fluxes of trace gases, Atmos. Environ., 30, 3321–3329, 1996.

Meyers, T. P., Luke, W. T., and Meisinger, J. J.: Fluxes of ammonia and sulfate over maize using relaxed eddy accumulation, Agr. Forest Meteorol., 136, 203–213, 2006.

Milne, R., Beverland, I. J., Hargreaves, K., and Moncrieff, J. B.: Variation of the β coefficient in the relaxed eddy accumulation method, Bound.-Lay. Meteorol., 93, 211–225, 1999.

Milne, R., Mennim, A., and Hargreaves, K.: The value of the beta coefficient in the relaxed eddy accumulation method in terms of fourth-order moments, Bound.-Lay. Meteorol., 101, 359–373, 2001.

Moravek, A., Trebs, I., and Foken, T.: Effect of imprecise lag time and high-frequency attenuation on surface–atmosphere exchange fluxes determined with the relaxed eddy accumulation method, J. Geophys. Res.-Atmos., 118, 10210–10224, 2013.

Obrist, D., Conen, F., Vogt, R., Siegwolf, R., and Alewell, C.: Estimation of Hg^0 exchange between ecosystems and the atmosphere using ^{222}Rn and Hg^0 concentration changes in the stable nocturnal boundary layer, Atmos. Environ., 40, 856–866, 2006.

Olofsson, M., Ek-Olausson, B., Jensen, N. O., Langer, S., and Ljungström, E.: The flux of isoprene from a willow plantation and the effect on local air quality, Atmos. Environ., 39, 2061–2070, 2005a.

Olofsson, M., Sommar, J., Ljungstrom, E., Andersson, M., and Wängberg, I.: Application of relaxed eddy accumulation technique to quantify Hg^0 fluxes over modified soil surfaces, Water Air Soil Pollut., 167, 331–352, 2005b.

Panofsky, H. A. and Dutton, J. A.: Atmospheric Turbulence – Models and Methods for Engineering Applications, Wiley, New York, 397 pp., 1984.

Peichl, M., Sagerfors, J., Lindroth, A., Buffam, I., Grelle, A., Klemedtsson, L., Laudon, H., and Nilsson, M. B.: Energy exchange and water budget partitioning in a boreal minerogenic mire, J. Geophys. Res.-Biogeo., 118, 1–13, 2013.

Pierce, A. M., Moore, C. W., Wohlfahrt, G., Hörtnagl, L., Kljun, N., and Obrist, D.: Eddy covariance flux measurements of gaseous elemental mercury using cavity ring-down spectroscopy, Environ. Sci. Technol., 49, 1559–1568, 2015.

Rannik, U., Aubinet, M., Kurbanmuradov, O., Sabelfeld, K. K., Markkanen, T., and Vesala, T.: Footprint analysis for measurements over a heterogeneous forest, Bound.-Lay. Meteorol., 97, 137–166, 2000.

Ren, X., Sanders, J. E., Rajendran, A., Weber, R. J., Goldstein, A. H., Pusede, S. E., Browne, E. C., Min, K.-E., and Cohen, R. C.: A relaxed eddy accumulation system for measuring vertical fluxes of nitrous acid, Atmos. Meas. Tech., 4, 2093–2103, doi:10.5194/amt-4-2093-2011, 2011.

Richardson, A. D., Aubinet, M., Barr, A. G., Hollinger, D. Y., Ibrom, A., Lasslop, G., and Reichstein, M.: Uncertainty quantification, in: Eddy Covariance – a Practical Guide to Measurement and Data Analysis, edited by: Aubinet, M., Vesala, T., and Papale, D., Springer Science + Business Media B.V., Dordrecht, the Netherlands, 173–209, 2012.

Sagerfors, J., Lindroth, A., Grelle, A., Klemedtsson, L., Weslien, P., and Nilsson, M.: Annual CO_2 exchange between a nutrient-poor, minerotrophic, boreal mire and the atmosphere, J. Geophys. Res.-Biogeo., 113, G01001, doi:10.1029/2006JG000306, 2008.

Schröder, W. H., Lindquist, O., and Munthe, J.: Volatilisation of mercury from natural surfaces, Proc. 7th International Conference of Heavy Metals in the Environment, Geneva, Switzerland, September 1989, edited by: Vernet, J. P., CEP Consultants, Edinburgh, UK, 480–484, 1989.

Schröder, W. H., Anlauf, K. G., Barrie, L. A., Lu, J. Y., Steffen, A., Schneeberger, D. R., and Berg, T.: Arctic springtime depletion of mercury, Nature, 394, 331–332, 1998.

Shanley, J. B. and Bishop, K.: Mercury cycling in terrestrial watersheds, in: Mercury in the Environment: Pattern and Process, 1st edn., edited by: Bank, M. S., University of California Press, Berkely, CA, 119–141, 2012.

Skov, H., Brooks, S. B., Goodsite, M. E., Lindberg, S. E., Meyers, T. P., Landis, M. S., Larsen, M. R. B., Jensen, B., McConville, G., and Christensen, J.: Fluxes of reactive gaseous mercury measured with a newly developed method using relaxed eddy accumulation, Atmos. Environ., 40, 5452–5463, 2006.

Slemr, F., Brunke, E.-G., Ebinghaus, R., Temme, C., Munthe, J. Wängberg, I., Schroeder, W., Steffen, A., and Berg, T.: Worldwide trend of atmospheric mercury since 1977, Geophys. Res. Lett., 30, 1516, doi:10.1029/2003GL016954, 2003.

Sommar, J., Zhu, W., Shang, L., Feng, X., and Lin, C.-J.: A whole-air relaxed eddy accumulation measurement system for sampling vertical vapour exchange of elemental mercury, Tellus B, 65, 19940, doi:10.3402/tellusb.v65i0.19940, 2013a.

Sommar, J., Zhu, W., Lin, C.-J., and Feng, X.: Field approaches to measure Hg exchange between natural surfaces and the atmosphere – a review, Critical Reviews in Environ. Sci. Technol., 43, 1657–1739, 2013b.

Steffen, A., Schroeder, W. H., Bottenheim, J., Narayan, J., and Fuentes, J. D.: Atmospheric mercury concentrations: measurements and profiles near snow and ice surfaces in the Canadian Arctic during Alert 2000, Atmos. Environ., 36, 2653–2661, 2002.

Sutton, M. A., Milford, C., Nemitz, E., Theobald, M. R., Hill, P. W., Fowler, D., Schjoerring, J. K., Mattsson, M. E., Nielsen, K. H., Husted, S., Erisman, J. W., Otjes, R., Hensen, A., Mosquera,

J., Cellier, P., Loubet, B., David, M., Genermont, S., Neftel, A., Blatter, A., Herrmann, B., Jones, S. K., Horvath, L., Fuhrer, E. C., Mantzanas, K., Koukoura, Z., Gallagher, M., Williams, P., Flynn, M., and Riedo, M.: Biosphere-atmosphere interactions of ammonia with grasslands: Experimental strategy and results from a new European initiative, Plant and Soil, 228, 131–145, 2001.

United Nations Environment Programme: Minimata Convention on Mercury, available at: http://www.mercuryconvention.org (last access: 10 January 2016), 62 pp., 2013a.

United Nations Environment Programme: Global Mercury Assessment 2013: Sources, Emissions, Releases and Environmental Transport, UNEP Chemicals Branch, Geneva, Switzerland, 42 pp., 2013b.

Walcek, C., De Santis, S., and Gentile, T.: Preparation of mercury emissions for eastern North America, Environ. Pollut., 123, 375–381, 2003.

Wallschläger, D., Turner, R. R., London, J., Ebinghaus, R., Kock, H. H., Sommar, J., and Xiao, Z. F.: Factors affecting the measurement of mercury emissions from soils with flux chambers, J. Geophys. Res.-Atmos., 104, 21859–21871, 1999.

Won, J. H., Park, J. Y., and Lee, T. G.: Mercury emissions from automobiles using gasoline, diesel, and LPG, Atmos. Environ., 41, 7547–7552, 2007.

Zhu, W., Sommar, J., Lin, C.-J., and Feng, X.: Mercury vapor air–surface exchange measured by collocated micrometeorological and enclosure methods – Part I: Data comparability and method characteristics, Atmos. Chem. Phys., 15, 685–702, doi:10.5194/acp-15-685-2015, 2015a.

Zhu, W., Sommar, J., Lin, C.-J., and Feng, X.: Mercury vapor air–surface exchange measured by collocated micrometeorological and enclosure methods – Part II: Bias and uncertainty analysis, Atmos. Chem. Phys., 15, 5359–5376, doi:10.5194/acp-15-5359-2015, 2015b.